ACS APPLIED MATERIALS & INTERFACES

Research Article

www.acsami.org

# Nanofluidic Diode Based on Branched Alumina Nanochannels with Tunable Ionic Rectification

Yan Kong,[†] Xia Fan,*[,†] MingHui Zhang,[†] Xu Hou,[‡] ZhaoYue Liu,[†] Jin Zhai,*[,†] and Lei Jiang[†]

[†]Key Laboratory of Bio-Inspired Smart Interfacial Science and Technology of Ministry of Education, School of Chemistry and Environment, Beihang University, Beijing 100191, P. R. China

[‡]National Center for Nanoscience and Technology, Beijing 100190, P. R. China

Supporting Information

**ABSTRACT:** In this work, the synthetic alumina nanochannels with bi-, tri-, and tetra-branched geometry structures exhibited ionic current rectifications with nonlinear $I-V$ curves. Such diode performance of the branched alumina nanochannel is mainly dependent on the cooperative asymmetry of the branched structure and the surface-charge distribution on inner walls. By regulating the geometry, electrolyte pH, and solution concentration, the tunable ionic rectification properties are effectively obtained including both the rectification ratios and the rectifying direction that were deduced from the converted ion selectivity. This nanofluidic diode may open up a new opportunity for the application of the complex nanofluidic devices in contrast to previously reported channels to provide molecular analysis, controlled mass transport, drug release, and various logic gate operations.

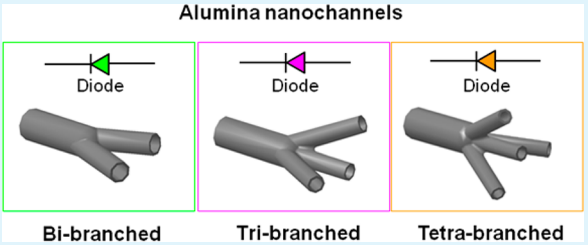


**KEYWORDS:** *nanofluidic diode, branched alumina nanochannel, tunable ionic rectification, pH, concentration, cooperative asymmetry*

## 1. INTRODUCTION

The biological ion channel that exists in living organisms plays an important role for regulating the flow of ions across the cell boundaries and providing the basis for maintaining cellular homeostasis.[1−3] Recently, inspired by biological channels, an artificial nanochannel that displays an ionic rectifying effect[4−8] like a liquid diode has attracted the wide attention of many researchers for their potential applications as building blocks for nanofluidic devices. Compared with polymer-based nanochannels,[9−12] inorganic nanochannels[13,14] have exhibited their particular advantages, such as repeatability and mechanical or chemical stability. Using electroless plating technology, Au nanochannels[15] have been reported with well-defined asymmetric pore geometry. Glass nanochannels[16] could be easily functionalized for the hydroxyl-terminated surface. SiN nanopores[17] fabricated on a Si substrate provided the possibility to integrate with other electronic devices. However, these nanochannels are not suitable for large scale application due to the complicated preparation processes or their disordered pore nature. Alumina nanochannels are becoming a desired candidate with ordered pores, high pore densities, and flexibility in controlling the geometry. Conventional cylindrical-shaped alumina nanochannels have been used for the applications in many areas such as biosensing, separation, and on−off gating[18,19] under external stimuli, including temperature,[20] ligand,[21] and light,[22] etc.

Structural parameters such as asymmetric shape and nanosized opening as well as surface charge have significant influences on the properties of nanofluidic diodes, and extensive efforts have been expended on controlling these two factors during synthesis and modification. To date, shape control typically relies on constructing an asymmetric conical nanochannel and its derivate.[23−25] Another approach is to introduce asymmetric chemical components on walls of symmetric nanochannels.[26−30]

This makes possible branched alumina nanochannel rectify ionic current because branched nanochannel has the natural presence of intrinsic asymmetric structure that composed of a stem and several connected branch segments. In previous research, branched nanochannels have been extensively used as a template in nanofabrication.[31,32] Smirnov and co-workers also demonstrated the different volume exclusion effect between two opening sides that was applied for sensing DNA hybridization based on a 20 nm/200 nm alumina nanoporous bounded electrode.[33] However, the branched conditions of these commercial nanochannels have not been exactly described and the thickness of the branch segment is only 1 $\mu$m, which does not benefit ion transportation controlling. Until now, there is no report about ionic rectification properties based on branched alumina nanochannels. Unlike previously reported heterogeneous nanochannel systems using alumina with a uniform distribution that typically rely on complicated and expensive physical fabrication methods, such as atomic layer deposition,[34] photolithography,[35] and reactive ion etching,[36] branched alumina nanochannels with a tunable asymmetric geometry in terms of branch numbers and pore

Received: May 24, 2013
Accepted: July 11, 2013
Published: July 11, 2013

   dx.doi.org/10.1021/am402004k | ACS Appl. Mater. Interfaces 2013, 5, 7931−7936

diameters can be designed and easily controlled during the fabrication process. More recently, Xia et al. prepared an amine group patterned alumina nanochannel array for constructing asymmetric surface charge distribution in a uniform nanochannel using a combination of synthesis and modification processes.[37] In this work, we demonstrated for the first time that, without any modification or heterogeneous materials, the synthetic alumina nanochannels with bi-, tri-, and tetra-branched geometry structures exhibited current rectifications, as well as a geometry-modulated performance. Such diode behavior of a branched nanochannel can be attributed to the cooperative asymmetry of the geometry and the surface-charge distribution at designed position. Furthermore, pH-reversed and electrolyte-concentration-responsive ionic-current rectification of branched alumina nanochannels was realized.

## 2. EXPERIMENTAL SECTION

**2.1. Alumina Nanochannel Fabrication.** Alumina nanochannels were fabricated via the modified two-step anodization process as the reported approach.[31,32] The number of branches can be controlled by tuning anode voltages. High-purity aluminum foil was used as the anode with a graphite plate as the counter electrode. The first anodization process was the same for all products. Aluminum foils were anodized under a voltage of 50 V for 4 h. As an electrolyte, a 0.3 M oxalic acid solution was used and the temperature was kept constant within 5 ± 1 °C. The resulting porous-oxide layer was then removed in a 0.5 M phosphoric acid/0.2 M chromic acid mixture at 60 °C for 15 min. In the second anodization process, we regulated the anodizing voltage to control the formation of branched channels. Initially, the anodization was performed under the same conditions as those in the first step for 2 h to create the primary channel segment. Without changing the anodizing voltage in a further synthesis process, an alumina single nanochannel membrane was obtained. When the anodized voltage is reduced, the dissolution of the barrier layer at the bottom of the stem channels dominates in the fabrication process and new cavities with small pore diameters will form. When the thickness of the barrier layer is reduced to a critical value, the anodizing continues and the controlled growth of branched channels was completed. Because the pore diameter is proportional to the anodization voltage, reducing the voltage by a factor of $1/\sqrt{n}$ results in $n$ times as many pores appearing in order to maintain the original total area of the oxide layer, and nearly all stem pores branched into the corresponding smaller-diameter pores. Here, $n$ represents the number of the branches split from that primary stem. In our work, anodized voltage was gradually reduced to 35, 28, or 25 V and the final channel segments for forming bi-, tri-, or tetra-branched alumina nanochannels were synthesized, respectively. The thickness of each nanochannel membrane is the same, which is controlled independently by the corresponding anodization time. For fabricating the tetra-branched alumina nanochannel, sulfuric acid electrolyte solution was introduced. Finally, the residual aluminum substrate was removed with saturated copper dichloride solution. As-fabricated alumina nanochannels with different geometrical structure were characterized with a field-emission scanning electron microscope (FE-SEM, Hitachi, S4300).

**2.2. Nanofluidic Diode Performance Measurements.** The alumina nanochannel membrane was mounted between two halves of an electrochemical cell, as shown in Figure S1 (Supporting Information). Each cell was filled with potassium chloride solution with the same concentration. The pH of the electrolyte would be adjusted with 1 M hydrochloric acid or potassium hydroxide solution. Ag/AgCl electrodes were settled in each half-cell to apply the desired transmembrane potential and to measure the resulting ionic current. $I-V$ curves were measured using a Keithley 6487 picoammeter/voltage source. The voltage was stepped between −0.2 V and +0.2 V with 20 mV steps, lasting 5 s. In our experiment, the anode faced the stem end and the cathode faced the branch end of nanochannels.

## 3. RESULTS AND DISCUSSION

**3.1. Microstructure and Morphology of Alumina Nanochannels.** Figure 1 shows the equivalent circuit components and the representative schematic diagrams of as-fabricated alumina nanochannels with a single nanofluidic diode nanochannel, respectively. SEM images of the final opening end of the nanochannels indicate that alumina nanochannels consist of closely packed, highly ordered pores. Without changing the anodizing voltage during the fabrication process, an alumina single nanochannel array that has a symmetric geometry structure was obtained (Figure 1a). SEM images of the primary opening end are characterized in Figure S2 (see the Supporting Information). The pore diameters of the single nanochannel array are about 80 ± 3 nm at both opening ends. The equivalent circuit component of the alumina single nanochannel is modeled as a resistor−capacitor (RC) connection. Here, the resistor represents the resistance of the nanochannel membrane. The capacitor stands for the impedance of the electrical double layer that is caused by the electrostatic interaction between ions and the charged inner wall. With gradually reducing anodizing voltage, bi- (Figure 1b), tri- (Figure 1c), and tetra-branched (Figure 1d) alumina nanochannel arrays were fabricated. Branched alumina nanochannels have an asymmetric geometry structure. In schematic diagrams, the branch segments are marked with dashed rectangles. As expected, branched nanochannels have the same pore diameters at the stem opening end as that of the single nanochannel. The pore diameters at branch ends are about 59 ± 3 nm (bibranched channel), 45 ± 3 nm (tribranched channel), and 30 ± 3 nm (tetra-branched channel), respectively. Therefore, with increasing number of branches, the pore diameters at the branch opening ends decrease in sequence. The cross-sectional SEM images in Figure S3 (Supporting Information) at low and high resolution reveal that all as-fabricated alumina nanochannel membranes have nearly the same thickness of about 50 $\mu$m and the lengths of the branch segments are about 20 $\mu$m.

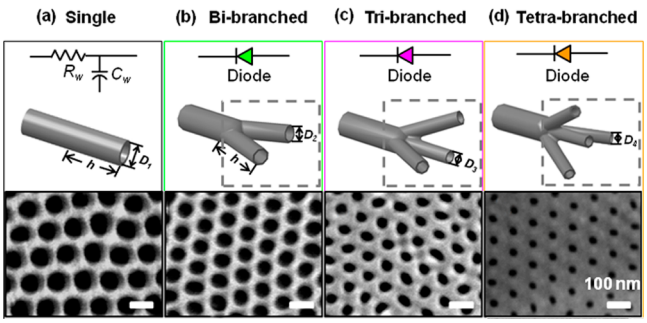


**Figure 1.** Equivalent circuit components, schematic diagrams, and SEM images of the final opening end (scale bar is 100 nm) of the as-prepared (a) alumina single nanochannel, (b) bibranched alumina nanochannel, (c) tribranched alumina nanochannel, and (d) tetra-branched alumina nanochannel. With increasing number of branches, the pore diameters at the branch opening end decreased.

**3.2. Influence of Geometry Structure, pH, and Concentration on the Nanofluidic Diode Performances.** Ionic rectifying properties of as-fabricated alumina nanochannel membranes were experimentally investigated by current−voltage ($I-V$) measurement, as shown in Figure 2a. All measurements were recorded under symmetric electrolyte solution of 0.1 mM KCl at pH 9.3 because the isoelectric

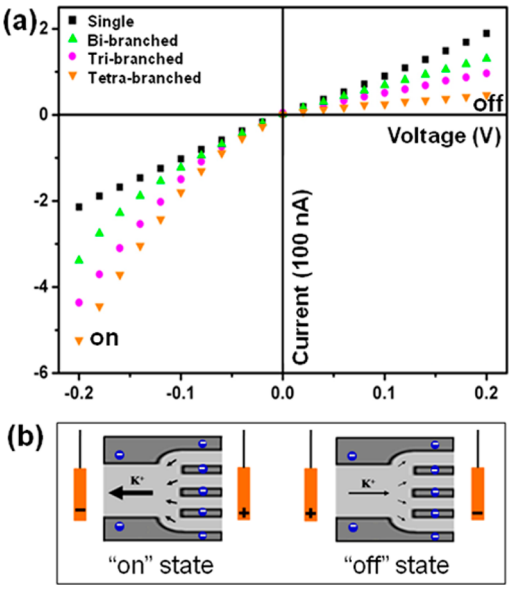


**Figure 2.** (a) $I-V$ curves of as-prepared alumina nanochannel membranes are in the following order: single nanochannels (■, black), bibranched nanochannels (▲, green), tribranched nanochannels (●, purple), and tetra-branched nanochannels (▼, orange). (b) Schematic representation of how the nanofluidic diode operates with tetra-branched alumina nanochannels as the model when the inner wall of channels was negatively charged. At positive voltage, the channels are the "off" state, while, at negative voltage, the channels are the "on" state. The current direction of the diode in "on" state is from the branch to the stem side. All measurements were recorded under symmetric electrolyte conditions at pH 9.3 and 0.1 mM KCl.

point (pI) of alumina is about 8.5,[38] which provided the inner wall of channels negatively charged surface with Al−O$^-$ terminated. Undoubtedly, the single alumina nanochannel array exhibits a linear $I-V$ curve, which means it does not rectify. Here, the electrostatic interaction inside the nanochannel is negligible. There is no ionic selective transport in symmetrical alumina nanochannels. The branched alumina nanochannel array exhibited ion current fluctuations of similar properties as the ion flow through biological voltage-gated channels. The effect of the asymmetry of electrical conductivity is well expressed even in cases when the pore diameter is substantially greater than the Debye length.[39−41] The ionic current rectification of branched alumina nanochannels was obviously observed as nonlinear $I-V$ curves with a controllable and continuous change. From bibranched to tetra-branched alumina nanochannels, current at negative voltages remarkably increased, while it decreased at positive voltage in sequence. Unlike previously reported systems that the small opening is on a scale of 10 nm, here the branched system can rectify ion current with a large opening because the thickness of the electric double-layer of alumina is larger than that of organic material.[42−44] Figure 2b illustrates how the rectifier operates with tetra-branched alumina nanochannels as the model. When the inner wall of channels was negatively charged, branched nanochannels would rectify the current with the preferential transport of the cation ($K^+$) flow. When the anode was placed at the stem opening end, larger currents would be exhibited at negative voltage (left in Figure 2b) than that at the opposite voltage (right in Figure 2b) with the same absolute value. Thus, at negative voltage, the channels are the "on" state, while, at positive voltage, the channels are relatively the "off" state. The branched alumina nanochannel array exhibited a diode-like property with the preferential current direction at the "on" state from the branch to the stem opening end when the inner surface was negatively charged.

The tunable current rectification behavior of as-fabricated alumina nanochannels is quantified by the membrane resistance (Figure 3a) and the current rectification ratios of on-state versus off-state (Figure 3b). The resistance of the single alumina nanochannel membrane is about $1.0 \times 10^6$ Ω at ±0.2 V. However, branched alumina nanochannel membranes possess a higher resistance when the $K^+$ is driven from the stem to the branch than from the branch to the stem, although the electrolyte in contact with the two pore openings is the same. The asymmetric resistance of the branched alumina nanochannel allowed the system to exhibit current rectification. There is a continued change of resistance with increasing branch number of alumina nanochannels that dramatically increases at +0.2 V but slightly decreases at −0.2 V. Therefore, the ionic-current rectification ratio at 0.1 and 0.2 V (red and blue) increased correspondingly. The ratio of the absolute values of ionic currents recorded at −0.2 and +0.2 V is approximately 2.7 in the bibranched nanochannel, while it is close to 12 in the tetra-branched alumina nanochannel. It is affirmative that one of the key factors to obtain the tunable rectification property is the controllable asymmetry structure.

Since alumina is an amphoteric material, we investigated the influence of the surface charge inside the nanochannel on diode behavior. By regulating the pH value of the electrolyte, the current rectification effect of the branched alumina nano-

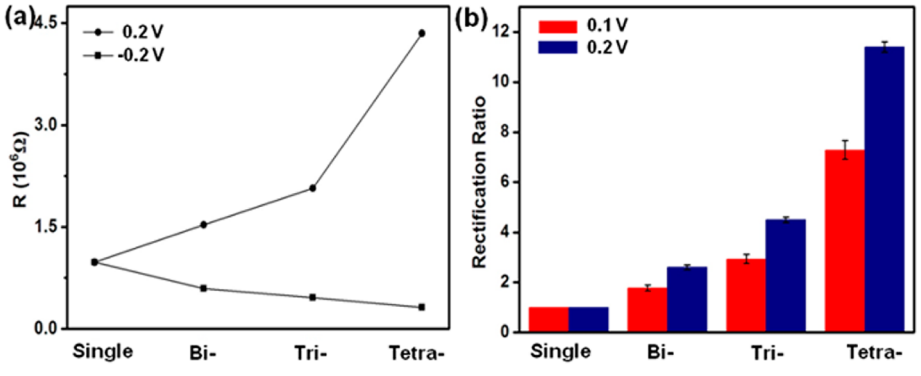


**Figure 3.** (a) The resistances of as-fabricated alumina nanochannel membranes were illustrated at +0.2 V (●) and −0.2 V (■). (b) Ion current rectification ratio of "on" state versus "off" state at 0.1 and 0.2 V (red and blue) of alumina naochannel with and without branched structures.

channel was converted as shown in Figure 4. $I-V$ curves of tetra-branched alumina nanochannels were recorded at different pH values. As measured above, alumina has an overall negatively charged surface at high pH values (pH 9.3). The nanochannel is now selective to cation, which allows mainly $K^+$ to transfer from the branch to the stem opening end. Conversely, at low pH values from 5 to 7, the alumina nanochannel becomes positively charged due to protonation ($Al-OH_2^+$ terminated). In this case, $Cl^-$ is the majority carrier, which is driven from the branch to the stem opening side and the preferential current direction is reversed. The nanochannel "on" (bottom right inset) and "off" states appear at positive voltage and negative voltage, respectively. However, no rectification behavior was measured at pH 8.5, which is close to the pI of alumina material.[38] At this pH value, the nanochannel net charge is zero (Al−OH terminated) and the $I-V$ curve shows a linear, nearly ohmic behavior. The nanochannels become nonselective. Thus, the pH-reverted surface behavior of branched alumina channels performed selective transport either cation or anion with that leading to the reversed current direction.

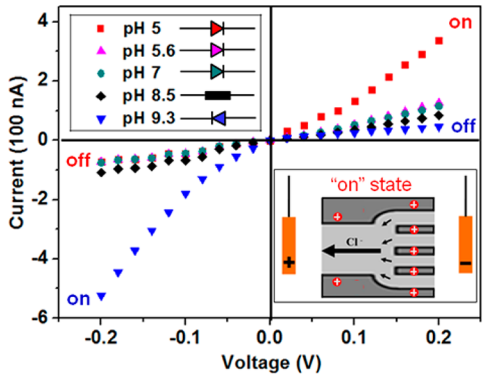


**Figure 4.** $I-V$ curves of tetra-branched alumina nanochannels recorded at pH ~ 5 (■), pH ~ 5.6 (▲), pH ~ 7 (●), pH ~ 8.5 (◆), and pH ~ 9.3 (▼) in 0.1 mM KCl. The current rectification effect is converted by regulating the value of electrolyte pH. When the branched nanochannel was positively charged at pH values from 5 to 7, the current direction of the diode in "on" state is from the stem to the branch side. At the same time, the inset shows the schematic of anion selective transport. A linear $I-V$ curve was measured at pH 8.5 near the pI of the alumina material.

In order to reveal the effect of the interaction between charged walls and ions in solution, the concentration-dependent rectification property of tetra-branched alumina nanochannels was investigated (Figure 5). Although the current amplitude increased monotonously with concentration, the rectification effect of the branched nanochannel decreased. Clearly, asymmetric $I-V$ curves would be measured at low concentrations, 0.1 mM (Figure 5a) and 10 mM (Figure 5b), respectively. Increasing the $K^+$ concentration to 0.1 M (Figure 5c) caused the $I-V$ curve to become linear. This is attributed to the formation of a diffuse electrical double layer within the branches. In highly concentrated solutions, the electrical double layer becomes too thin for ion current rectification to occur. In all cases, a pH of 9.3 is used, which offers the interaction between the negative surface charge on the inner wall and the ions in solution. The results show the importance of branched alumina nanochannels that allow exhibiting the good rectifying behavior at the dilute solution, which is different from organic nanochannels where the maximum rectification ratio was usually obtained near 0.1 M.[4] Thus, a nanofluidic diode device may be constructed for the detection of ions or charged molecules at low concentration using branched alumina channels as one of the candidates.

Geometric structure and surface charge cooperative asymmetry is the major effect determining the diode performance of the branched alumina nanochannel, which is detailed in Figure 6a. Here, the pore diameter, inner volume, surface area of inner walls, and surface to volume ratio of the final channel segment are recorded as $D_n$, $(V_w)_n$, $(S_w)_n$, and $(R_{s/v})_n$, respectively. Here, $n$ represents the number of branches split from that primary stem. Ratio curves of these parameters between branched channels to a single channel are represented in the following order: $D_n/D_1$, $(V_w)_n/(V_w)_1$, $(S_w)_n/(S_w)_1$, and $(R_{s/v})_n/(R_{s/v})_1$. The pore diameter is proportional to the anodizing voltage. From single channel to tribranched nanochannel, $D_n$ decreases following the ratio $1/\sqrt{n}$. Thus, derived from formulas 1 and 2, the values of $(V_w)_n$ have no change, while $(S_w)_n$ increases with the ratio $\sqrt{n}$ from single to tribranched nanochannel, where $h$ represents the length of the branch segment, as shown in Figure 1. It is noted that the tetra-branched nanochannel has the smallest pore diameter and inner volume in all products because the smallest anodizing voltage as well as sulfuric acid solution was used in fabricating it.

$$(V_w)_n = n\pi(D_n/2)^2 h \quad (1)$$

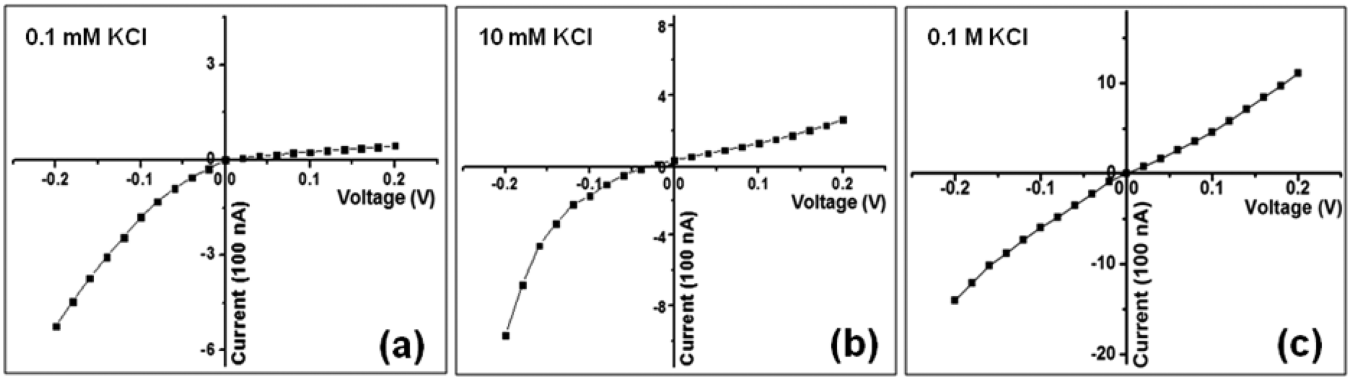


**Figure 5.** $I-V$ curves of tetra-branched alumina nanochannels recorded in (a) 0.1 mM KCl, (b) 10 mM KCl, and (c) 1 M KCl. The pH of electrolyte solution is 9.3.

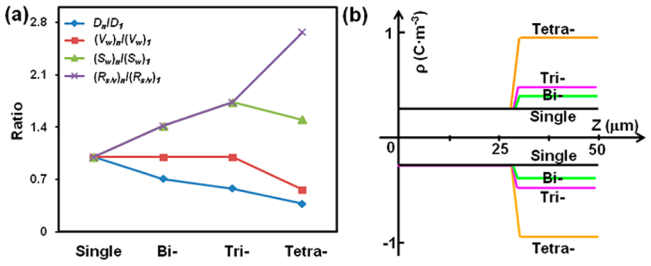


**Figure 6.** (a) Pore diameter $(D_n)$, inner volume $((V_w)_n)$, surface area of inner walls $((S_w)_n)$, and surface to volume ratio $((R_{s/v})_n)$ of the final channel segment were used to justify that structure and surface charge cooperative asymmetry is the major effect dictating the ionic rectifying behavior of branched alumina nanochannels. Ratio curves of these parameters between branched channels to single are represented in the following order: $D_n/D_1$ (◆, blue curve), $(V_w)_n/(V_w)_1$ (■, red curve), $(S_w)_n/(S_w)_1$ (▲, green curve), and $(R_{s/v})_n/(R_{s/v})_1$ (×, purple curve). (b) The relative distribution of surface-charge density $(\rho)$ of alumina nanochannels.

$$(S_w)_n = n\pi D_n h \quad (2)$$

Therefore, the surface to volume ratio dramatically increases from single channels to tetra-branched nanochannels. Thus, an asymmetric surface-charge distribution is exhibited on inner walls of branched alumina nanochannels. The relative distribution of the surface-charge density $(\rho)$ of the alumina nanochannel is presented in Figure 6b. Here, $Z$ presents the distance away from the stem opening end, which is along the channel direction and does not exceed the length of the nanochannels. The branch segment has a relatively higher absolute value of $\rho$ than that of the stem segment whether it possesses the positive or negative surface charges on walls. In addition, the role of the electric double layer in regulating ion transport is higher in narrower nanochannels. Asymmetric interaction between charged walls on branched nanochannels and ions in solution occurs, which results in the rectification of the ionic current of the branched nanochannel. Since $\rho$ and the electrostatic interaction increase from bibranched channel to tetra-branched channel at the branch segment, a higher asymmetric surface charge distribution along the nanochannel results in a higher rectification ratio. As measured, the current rectification ratios increase correspondingly. Here, the rectification ratio of the branched alumina nanofluidic diode is the same order of magnitude as that for other unipolar diodes. The diode performance could be enhanced by further decreasing the pore diameters of the nanochannels at both stem and branch segments.[37]

## 4. CONCLUSIONS

We have fabricated nanofluidic diodes based on bi-, tri-, and tetra-branched alumina nanochnanel arrays and experimentally demonstrated the tunable rectification effects, which were effectively regulated by the geometry, electrolyte pH, and solution concentration. The diode performance of the branched alumina nanochannel is mainly dependent on the cooperative asymmetric effect of the branched structure and the surface-charge distribution on inner walls. Compared with other nanofluidic diodes, branched alumina nanochannels may open up a new opportunity for the development and application of more complex nanofluidic devices than what exists today to provide molecular analysis, controlled mass transport, and drug release. Furthermore, analogous to a diode in solid-state electronics, a branched alumina nanofluidic diode may be considered as a promising component for building logic circuit and amplifying circuit.

## ■ ASSOCIATED CONTENT

### Supporting Information

Schematic diagram of the experimental setup for $I-V$ measurement. SEM images of the primary opening end of the alumina single nanochannel. The cross-sectional SEM images of alumina single and bi-, tri-, and tetra-branched nancochannels. This material is available free of charge via the Internet at http://pubs.acs.org.

## ■ AUTHOR INFORMATION

### Corresponding Author

*E-mail: fanxia@buaa.edu.cn (X.F.); zhaijin@buaa.edu.cn (J.Z.).

### Notes

The authors declare no competing financial interest.

## ■ ACKNOWLEDGMENTS

We thank the National Natural Science Foundation of China (Grant No. 21101009 and Grant No. 20971010) and the National Basic Research Program of China (973 Program, Grant No. 2010CB934700). The work was also supported by the Research Fund for the Doctoral Program of Higher Education of China (Grant No. 20101102120051) and the Fundamental Research Funds for the Central Universities (Grant No. YWF-10-03-Q-088).

## ■ REFERENCES

(1) Hille, B. In *Ionic Channels of Excitable Membranes*, 3rd ed.; Sinauer Associates: Sunderland, MA, 2001; pp 1−21.
(2) Kühlbrandt, W. *Nat. Rev. Mol. Cell Biol.* **2004**, *5*, 282−295.
(3) Jasti, J.; Furukawa, H.; Gonzales, E. B.; Gouaux, E. *Nature* **2007**, *449*, 316−323.
(4) Siwy, Z. S. *Adv. Funct. Mater.* **2006**, *16*, 735−746.
(5) Wen, L. P.; Hou, X.; Tian, Y.; Zhai, J.; Jiang, L. *Adv. Funct. Mater.* **2010**, *20*, 2636−2642.
(6) Cheng, L. J.; Guo, L. J. *Chem. Soc. Rev.* **2010**, *39*, 923−938.
(7) Guo, Z. J.; Wang, J. H.; Ren, J. T.; Wang, E. K. *Nanoscale* **2011**, *3*, 3767−3773.
(8) Escosura-Muñiz, A.; de la Merkoçi, A. *ACS Nano* **2012**, *6*, 7556−7583.
(9) Han, C. P.; Hou, X.; Zhang, H. C.; Guo, W.; Li, H. B.; Jiang, L. *J. Am. Chem. Soc.* **2011**, *133*, 7644−7647.
(10) Zhang, M. H.; Hou, X.; Wang, J. T.; Tian, Y.; Fan, X.; Zhai, J.; Jiang, L. *Adv. Mater.* **2012**, *24*, 2424−2428.
(11) Yameen, B.; Ali, M.; Neumann, R.; Ensinger, W.; Knoll, W.; Azzaroni, O. *J. Am. Chem. Soc.* **2009**, *131*, 2070−2071.
(12) Ali, M.; Yameen, B.; Cervera, J.; Ramírez, P.; Neumann, R.; Ensinger, W.; Knoll, W.; Azzaroni, O. *J. Am. Chem. Soc.* **2010**, *132*, 8338−8348.
(13) Gyurcsányi, R. E. *Trends Anal. Chem.* **2008**, *27*, 627−639.
(14) Hou, X.; Guo, W.; Jiang, L. *Chem. Soc. Rev.* **2011**, *40*, 2385−2401.
(15) Harrell, C. C.; Siwy, Z. S.; Martin, C. R. *Small* **2006**, *2*, 194−198.
(16) Wang, G. L.; Bohaty, A. K.; Zharov, I.; White, H. S. *J. Am. Chem. Soc.* **2006**, *128*, 13553−13558.
(17) Vlassiouk, I.; Apel, P. Y.; Dmitriev, S. N.; Healy, K.; Siwy, Z. S. *Proc. Natl. Acad. Sci. U.S.A.* **2009**, *106*, 21039−21044.
(18) Kumar, S. K.; Hong, J. D. *Langmuir* **2008**, *24*, 4190−4193.
(19) Jiang, Y. N.; Liu, N. N.; Guo, W.; Xia, F.; Jiang, L. *J. Am. Chem. Soc.* **2012**, *134*, 15395−15401.

(20) Zhou, Y. H.; Guo, W.; Cheng, J. S.; Liu, Y.; Li, J. H.; Jiang, L. *Adv. Mater.* **2012**, *24*, 962−967.
(21) Steinle, E. D.; Mitchell, D. T.; Wirtz, M.; Lee, S. B.; Young, V. Y.; Martin, C. R. *Anal. Chem.* **2002**, *74*, 2416−2422.
(22) Li, S. J.; Li, J.; Wang, K.; Wang, C.; Xu, J. J.; Chen, H. Y.; Xia, X. H.; Huo, Q. *ACS Nano* **2010**, *4*, 6417−6424.
(23) Ramírez, P.; Apel, P. Y.; Cervera, J.; Mafé, S. *Nanotechnology* **2008**, *19*, 315707.
(24) Siwy, Z. S.; Howorka, S. *Chem. Soc. Rev.* **2010**, *39*, 1115−1132.
(25) Hou, X.; Dong, H.; Zhu, D. B.; Jiang, L. *Small* **2010**, *6*, 361−365.
(26) Hou, X.; Liu, Y. J.; Dong, H.; Yang, F.; Li, L.; Jiang, L. *Adv. Mater.* **2010**, *22*, 2440−2443.
(27) Hou, X.; Yang, F.; Li, L.; Song, Y. L.; Jiang, L.; Zhu, D. B. *J. Am. Chem. Soc.* **2010**, *132*, 11736−11742.
(28) Ali, M.; Ramirez, P.; Nguyen, H. Q.; Nasir, S.; Cervera, J.; Mafe, S.; Ensinger, W. *ACS Nano* **2012**, *6*, 3631−3640.
(29) Kalman, E. B.; Vlassiouk, I.; Siwy, Z. S. *Adv. Mater.* **2008**, *20*, 293−297.
(30) Karnik, R.; Duan, C.; Castelino, K.; Daiguji, H.; Majumdar, A. *Nano Lett.* **2007**, *7*, 547−551.
(31) Vlassiouk, I.; Takmakov, P.; Smirnov, S. *Langmuir* **2005**, *21*, 4776−4778.
(32) Yan, R. X.; Liang, W. J.; Fan, R.; Yang, P. D. *Nano Lett.* **2009**, *9*, 3820−3825.
(33) Cheng, L. J.; Guo, L. J. *ACS Nano* **2009**, *3*, 575−584.
(34) Wu, S. M.; Wildhaber, F.; Vazquez-Mena, O.; Bertsch, A.; Brugger, J.; Renaud, P. *Nanoscale* **2012**, *4*, 5718−5723.
(35) Li, C. Y.; Ma, F. X.; Wu, Z. Q.; Gao, H. L.; Shao, W. T.; Wang, K.; Xia, X. H. *Adv. Funct. Mater.* **2013**, DOI: 10.1002/adfm.201300315.
(36) Meng, G. W.; Jung, Y. J.; Cao, A. Y.; Vajtai, R.; Ajayan, P. M. *Proc. Natl. Acad. Sci. U.S.A.* **2005**, *102*, 7074−7078.
(37) Chen, B. S.; Xu, Q. L.; Zhao, X. L.; Zhu, X. G.; Kong, M. G.; Meng, G. W. *Adv. Funct. Mater.* **2010**, *20*, 3791−3796.
(38) Kosmulski, M. *J. Colloid Interface Sci.* **2004**, *275*, 214−224.
(39) Apel, P. Yu.; Blonskaya, I. V.; Levkovich, N. V.; Orelovich, O. L. *Petrol. Chem.* **2011**, *51*, 555−567.
(40) Umehara, S.; Pourmand, N.; Webb, C. D.; Davis, R. W.; Yasuda, K.; Karhanek, M. *Nano Lett.* **2006**, *6*, 2486−2492.
(41) Wei, C.; Bard, A. J. *Anal. Chem.* **1997**, *69*, 4627−4633.
(42) Schmid, G. *J. Membr. Sci.* **1998**, *150*, 151−157.
(43) Stern, O. *Z. Elektrochem. Angew. Phys. Chem.* **1924**, *30*, 508−516.
(44) Bluhm, E. A.; Bauer, E.; Chamberlin, R. M.; Abney, K. D.; Young, J. S.; Jarvinen, G. D. *Langmuir* **1999**, *15*, 8668−8672.